PERGAMON

International Journal of Solids and Structures 38 (2001) 6045–6061

INTERNATIONAL JOURNAL OF SOLIDS and STRUCTURES

www.elsevier.com/locate/ijsolstr

Dynamic characterization of layered and graded structures under impulsive loading

Y. Li [a], K.T. Ramesh [a,*], E.S.C. Chin [b]

[a] *Department of Mechanical Engineering, Laboratory for Impact Dynamics & Rheology, The Johns Hopkins University, 122 Latrobe Hall, 3400 N.Charles street, Baltimore, MD 21218, USA*

[b] *Army Research Laboratory, Weapons and Materials Research Directorate, Aberdeen Proving Ground, MD 21005, USA*

Received 14 February 2000

Abstract

Relatively thick graded and layered structures have significant potential armor applications, and have recently been manufactured with some degree of consistency. The mechanical behaviors of the individual layers within such a structure play an important role in determining the structure's resistance to impact. This work examines layered and graded plates made of metal–ceramic composites with the volume fraction of ceramic reinforcement varying through the thickness. In a previous work (Acta Mater 46 (1998) 5633), the results of high-strain-rate experiments have been used to develop a model for the viscoplastic response of metal–matrix composites of varying volume fraction. Using this model, numerical results are presented on the propagation of large amplitude stress waves through layered and graded structures. The results show that the wave propagation within layered and graded structures involves a complex coupling of elastic and viscoplastic response. It is demonstrated that the choice of gradation has great significance for impact applications.

Keywords: FGM; IMPACT; Stress wave; MMC

1. Introduction

Several different materials are often used in structural components in order to optimize the response of the structure to thermal and mechanical loading (e.g. thermal-barrier coatings). However, abrupt transitions in material properties may induce local stress concentrations within the structural component. These stress concentrations are often greatly reduced if the transition from one material to the other is made gradual, leading to the concept of functionally graded materials (FGMs). By definition, FGMs are used to produce components featuring engineered gradual transitions in microstructure and/or composition, motivated by performance requirements that vary with location within the parts. With FGMs, these requirements are met in a manner that optimizes the overall performance of the component. In the 'inverse design procedure,' the component design and fabrication are based on a choice of available basic material

* Corresponding author. Tel.: +1-410-516-7735; fax: +1-410-516-7254.
E-mail address: ramesh@jhu.edu (K.T. Ramesh).

0020-7683/01/$ - see front matter
PII: S0020-7683(00)00364-4

ingredients and material processes, combined with three-dimensional thermomechanical analysis of graded structures.

Over the last decade, great advancements have been made in research on FGMs with regard to both fabrication and applications (Miyamoto et al., 1996; Rodel and Neubrand, 1996; Ilschner, 1996). The micromechanics and physical principles for FGMs subjected to quasistatic loading are discussed by Mortensen and Suresh (1995) and Suresh and Mortensen (1997). Giannakopoulos and Suresh (1997a,b), conducted analytical and computational studies of the evolution of stresses and displacements due to indentation on an elastic substrate, the Young's modulus of which varies as a function of depth beneath the indented surface. Their results showed that the FGM response is sensitive to the variation of Poisson's ratio as well as to the variation of Young's modulus. Finot et al. (1996) studied the elastoplastic deformation characteristics of a plasma-sprayed, trilayered composite plate subject to thermal cycling from 20°C up to 800°C, and Finot and Suresh (1996) analyzed the thermomechanical response of multi-layered materials subjected to deformation during temperature excursions. The effects of the variation of Poisson ratio, layer geometry, plastic flow and compositional gradation were examined. Pettermann et al. (1996) and Weissenbek et al. (1997) analyzed the elastic–plastic deformation of Ni–Al_2O_3 layered systems using detailed finite element models with planar geometry and perfectly periodic arrangements of constituent phases. They found that square-packing arrangements provide the best possible bounds for the thermal strains and coefficient of thermal expansion; however, no unique bounds could be identified for mechanical load. The mean-field approach provided a stiffer mechanical response than the finite element unit cell models. The predicted stress and strain response depends strongly on the microarrangement of the inclusions. Reiter et al. (1997) and Reiter and Dvorak (1998) proposed micromechanical models for graded composite materials based on detailed finite element studies conducted using large plane-array domains containing simulated skeletal and particulate microstructures. Thermal residual stresses in graded ceramic metal interfaces and joints were analyzed by Williamson et al. (1993), Rabin et al. (1993), Ravichandran (1995), Yang and Munz (1995), and Yang and Munz [1996]. The conclusion is that the utilization and optimization of a graded interface layer between two dissimilar layers can reduce the stresses significantly; this is believed to be very important for controlling interface failure. Clearly, most of the above research works are concerned with thin film structures subjected to primarily thermal loading. To the authors' knowledge, there is little research concerning thick layered or graded structures under impulsive loading. This is the area of research with direct application to armor structures.

There is a clear driving force towards reducing the weight of armored weaponry in order to develop rapid response forces that can use air-lift capabilities. Considerable effort has been expended over the past two decades towards such an objective, with a significant effort directed towards ceramic armor. Advanced armor structures that combine the low weight and high hardness of ceramic armor with the toughness, damage tolerance, and low-cost manufacturability of metallic armor will clearly be of tremendous value. Entirely experimental ballistic evaluations of the efficiency of a graded armor structure designed on an ad hoc basis has shown that the hybrid materials approach to improved armor is of great potential benefit. The class of hybrid materials with graded/layered microstructures containing both ceramic and metallic phases is therefore of interest. The most straightforward form of graded microstructure consists of a gradation in the volume fraction of either the metal or ceramic phase, leading to either metal–matrix composites (MMCs) or ceramic–matrix composites (CMCs), with "monolithic" metals and ceramics at the two ends of the range.

This paper examines the impact response of layered and graded metal–ceramic structures using a computational approach. In the layered case, each individual layer is itself a MMC with a different volume fraction of reinforcement (up to about 60% ceramic content). In the graded case, smooth gradations of ceramic volume fraction across the thickness of the plate are considered. The effect of reinforcement volume fraction on the viscoplastic behavior is described using an experimentally verified analytical model presented by Li and Ramesh (1998). We are particularly concerned with the propagation of large amplitude

stress waves through such structures and with the identification of the failure mechanisms that may arise as a result of impulsive loading.

2. Graded/layered structures investigated

2.1. Geometric considerations

The geometry of interest is that of a circular cylindrical plate of thickness h and diameter $d \gg h$ (Fig. 1), which is impulsively loaded on the top surface, with the load applied along the axis over a radius a ($a < h$). It is assumed that the material of the plate is compositionally graded along the thickness direction, but that no gradations are developed along the radial direction. The gradation is developed in terms of the volume fraction of a ceramic reinforcing phase within a metal matrix. The mechanical response of this graded structure to an impulsive loading is of interest. The propagation of stress waves within the structure is key to this impulsive response, and this wave propagation creates timescales of interest to the analysis. The primary timescale is $t_0 = h/c_f$, where c_f is the speed of the fastest longitudinal wave in the system; this is the earliest time at which information from one face of the plate can arrive at the second face. A secondary timescale in the problem is given by $t_b = d/c_f$; this is the earliest time at which information from the circumferential boundaries of the plate is received at the plate axis. The plate is assumed to be fixed along the circumferential edges, so that an axisymmetric mode of deformation would result for axisymmetric loading. However, the times over which this analysis is developed are such that $t_0 \ll t_b$, so that the boundaries of the plate are not actually involved in these calculations. The physical dimensions of the plate used in this analysis are a diameter of 200 mm and a thickness of 24.5 mm. These dimensions were chosen because they represent typical size scales for graded structures that have actually been manufactured.

2.2. Graded structures

It is assumed that the material of the plate is a metal–ceramic composite with the ceramic particulate reinforcement volume fraction f varying along the thickness z, i.e. the reinforcement volume fraction is $f(z)$.

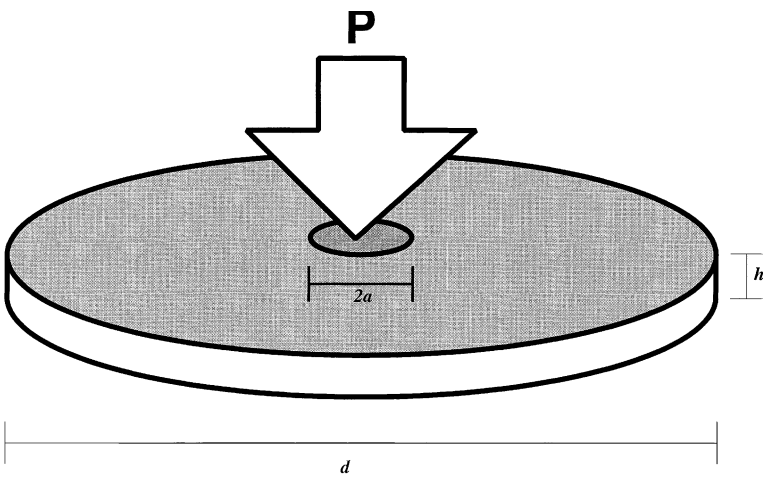

Fig. 1. Schematic of the geometry investigated in this paper. All of the gradations considered occur in the thickness direction of the plate.

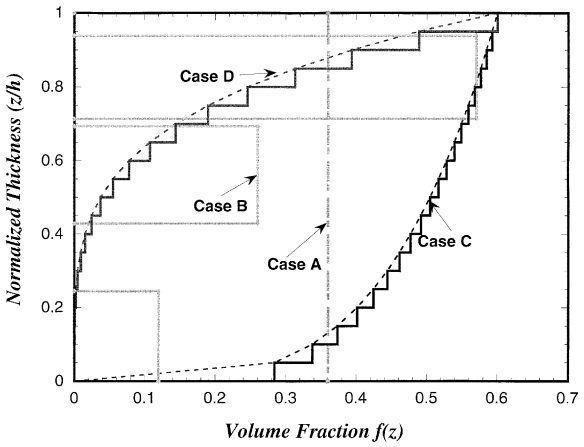

Fig. 2. The specific gradations investigated. The material of the plate is a metal–ceramic composite with the ceramic reinforcement volume fraction f varying along the thickness z, i.e. $f(z)$. Four possible forms of $f(z)$ are considered, corresponding to the cases described in the text.

Four possible forms of $f(z)$ are considered (Fig. 2). In the first case, (Case A), the plate is assumed to be composed of a single MMC with fixed volume fraction f_0, i.e., $f(z) = f_0$. Case B is a layered structure, with the reinforcement volume fraction jumping discontinuously from layer to layer, with the specific volume fractions for each layer chosen to match an experimental structure developed by MMCCI (described subsequently). The third and fourth cases considered (Cases C and D) involve reinforcement volume fractions that vary continuously with thickness following a power law:

$$f(z) = f_0\left(\frac{z}{h}\right)^b \tag{1}$$

where b is a parameter which defines the variation of reinforcement volume fraction. In these power-law graded structures the minimum reinforcement volume fraction ($f = 0$, or pure metal) occurs at one face of the plate, while the maximum reinforcement volume fraction ($f = f_0$) occurs at the other face of the plate. Note that $b = 0$ represents the homogeneous case (Case A), while $b = 1$ represents the case of linear variation of reinforcement volume fraction (this case is not considered here). Further, note that $b < 1$ and $b > 1$ represent markedly different gradations, particularly in terms of the degree to which the high-volume fractions are present at the impact face. Two specific continuous gradations are considered, with $b = 0.25$ for Case C and $b = 4$ for Case D.

A mean reinforcement volume fraction $\bar{f}$ may be defined for a given plate with such through-thickness gradations:

$$\bar{f} = \frac{1}{h}\int_0^h f(z)\mathrm{d}z \tag{2}$$

This mean volume fraction has the following values for the cases considered: Case A (uniform): $\bar{f} = 36\%$; Case B (layered): $\bar{f} = 22.6\%$; Case C (high f front): $\bar{f} = 47.5\%$; and Case D (low f front): $\bar{f} = 12\%$. These differences in mean reinforcement volume fraction must be considered when examining the effective compliances of these structures.

A summary of the graded structures investigated is presented in Table 1.

Table 1
Characteristics of the structures considered

Case	Description	$f(z)$	Parameters	Mean, $\bar{f}$
A	Uniform	f_0	$f_0 = 0.36$	0.360
B	Layered	$f_0, f_1, f_2, \ldots$	See Fig. 2	0.226
C	High f front	$f_0\left(\frac{z}{h}\right)^b$	$f_0 = 0.6$, $b = 0.25$	0.475
D	Low f front	$f_0\left(\frac{z}{h}\right)^b$	$f_0 = 0.6$, $b = 4.0$	0.120

2.3. Experimental layered armor structure

A layered structure consisting of seven layers with a total thickness of 24.5 mm was fabricated by MMCCI as a laboratory demonstrator for possible armor structures (a piece of this plate was kindly provided to us by the US Army Research Laboratory for characterization). Each individual layer is a metal–ceramic composite, consisting of an aluminum alloy reinforced by varying volume fractions of both ceramic whiskers and ceramic particles (Fig. 3). The nominal reinforcement volume fraction of each layer was (from bottom to top) 12%, 0%, 26%, 0%, 57% and 0%, with corresponding layer thicknesses of 6, 4.5, 6.5, 0.5, 5.5 and 1.5 mm respectively. For the layers with reinforcement volume fractions of 12% and 26%, the reinforcements consist of fine particle and whiskers; for the high reinforcement volume fraction layer with $f = 57\%$, the reinforcements consist of both large and fine particles and whiskers. The layers with 0% of the reinforcement represent the matrix alloy, which is essentially 6061-T6 aluminum alloy with a slightly different composition as a result of the processing route. The interfaces between the layers are not graded, so that the structure is a good example of the discontinuously layered case (Case B). Since this structure had already been fabricated, this specific volume fraction distribution was used for our investigations of the layered case. The specific values of f chosen for each layer are related to specific expectations for ballistic performance, but the rationale for these choices is beyond the scope of this paper.

3. Constitutive behaviors

The materials within these graded structures are all MMCs, with a contiguous metal phase (the maximum reinforcement volume fraction anywhere in these structures is less than 60%) and discontinuous ceramic reinforcements (idealized as particulates, even though some whiskers are present in the physical layered structure). These composites are assumed to behave as elastic/viscoplastic materials, with the effective properties of the composites obtained from models based on the mechanical properties of the

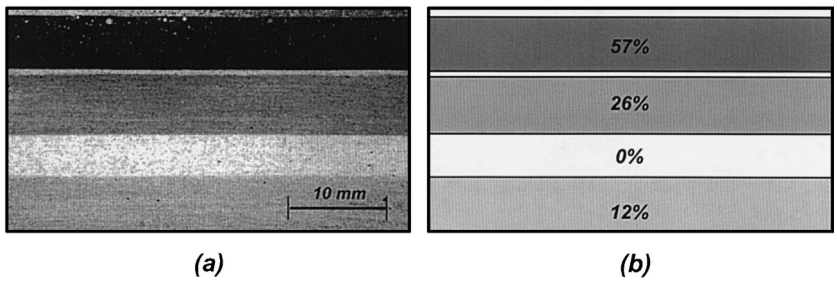

Fig. 3. Experimental layered structure fabricated by MMCCI: (a) optical micrograph (b) schematic of layering.

Table 2
The elastic properties of the metal matrix and ceramic reinforcement materials

Materials	Young's modulus (GPa)	Shear modulus (MPa)	Poisson's ratio	Density ($kg\,m^{-3}$)	Impedance ($kg\,m^{-2}\,s^{-1}$)
Matrix	70	26.9	0.3	2800	16.2×10^6
Ceramic	420	179.5	0.17	3200	38.0×10^6

individual phases and the reinforcement volume fraction (reinforcement shape and size effects are not considered). The elastic properties of the composites are estimated using the Hashin–Shtrikman method using the known elastic properties of the matrix and reinforcement phases (Table 2) and the known local volume fraction. The viscoplastic behavior of the composites are obtained using the analytical model developed by Li and Ramesh (1998):

$$\sigma\left(f,\varepsilon,\dot{\varepsilon}\right) = \sigma_0(\varepsilon)g(f)\left[1+\left(\frac{\dot{\varepsilon}}{\dot{\varepsilon}_0}\right)^m\right]\left[1+f\left(\frac{\dot{\varepsilon}}{\dot{\varepsilon}_0}\right)^m\right] \tag{3}$$

where $\sigma_0(\varepsilon)$ represents the stress–strain response of the matrix at quasistatic rates of deformation and is obtained directly from experiment. The strengthening function $g(f)$ represents the variation of the flow stress ratio with volume fraction f at quasistatic rates of deformation and is obtained from numerical calculations using unit cell models (as in Li and Ramesh (1998)). For this particular case, we assume this function to have the same form as that used by Li and Ramesh (1998):

$$g(f) = 1 + 1.17f + 2.28f^2 + 21.0f^3 \tag{4}$$

The parameters m and $\dot{\varepsilon}_0$ determine the rate dependence of the matrix material, and are extracted from experimental data that includes a wide range of strain rates.

The specific values for the various parameters in the viscoplastic constitutive function (3) were determined on the basis of the materials in the experimental layered structure. The matrix in the experimental layered structure is essentially 6061-T6 aluminum, with slight differences in composition as a result of the processing route. The rate-dependent parameters were obtained from the experimental data of Yadav et al. (1995) on 6061-T6 Al alloy, resulting in a reference strain rate $\dot{\varepsilon}_0$ of $1.4655 \times 10^5\ s^{-1}$ and a strain rate hardening exponent m of 0.045. The work hardening of the matrix is incorporated within $\sigma_0(\varepsilon)$ and is assumed to be independent of strain rate (known to be a good assumption for this matrix alloy). The last term in Eq. (3) represents the direct coupling of the strain-rate and volume fraction effects. This model has been shown to work with a number of similar particle-reinforced MMCs (Li and Ramesh (1998), Li et al. (2000a)). The composites in the experimental layered structure that we consider also include some whisker reinforcements, but we believe the use of this model will still provide insight into the qualitative features of the impact response in this case.

Fig. 4 summarizes the gradations in material properties that arise from the gradations in volume fraction shown in Fig. 2, using the elastic and viscoplastic models described in the preceding paragraphs. The variation of the Young's modulus with location along the thickness direction is shown in Fig. 4(a), and the variation of Poisson's ratio with thickness is shown in Fig. 4(b). The variation of the acoustic impedance (defined as ρc_l, where ρ is the local density and c_l is the local longitudinal wave velocity) through the thickness direction is presented in Fig. 4(c). Discontinuous changes in the acoustic impedance will cause wave reflections and thus dramatically influence the impact response of the structure. Finally, the variation of the yield stress with thickness is shown in Fig. 4(d) as computed using the model of Eq. (3); comparison with Fig. 2 demonstrates the strong influence of reinforcement volume fraction on the local flow stress. The primary observation from Fig. 4 is that the variation of reinforcement volume fraction can cause quite

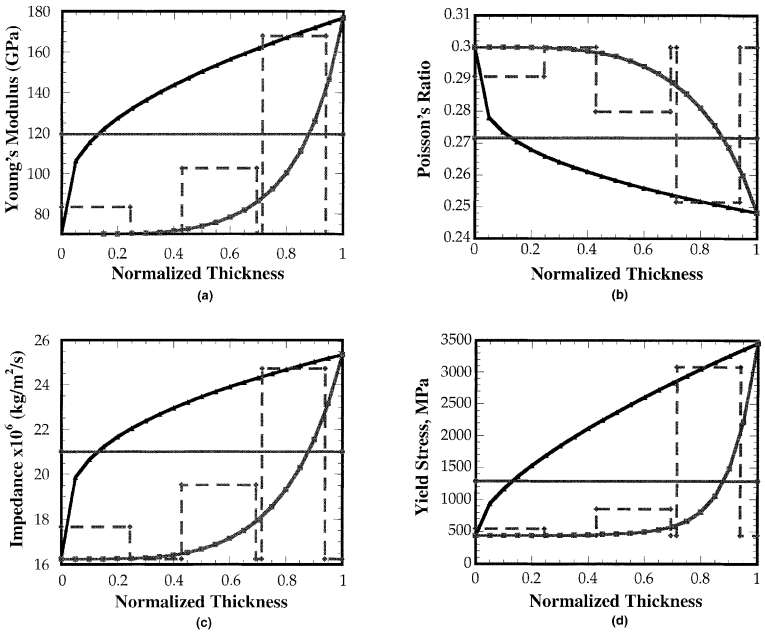

Fig. 4. Variation of properties for Cases A–D through the thickness of the plate, represented by the normalized thickness coordinate, z/h. (a) Young's modulus, (b) Poisson's ratio, (c) acoustic impedance and (d) yield stress under quasistatic loading. Note that the top surface of the plate is represented by the right-hand edge of the normalized thickness axis ($z = h$).

complex variations in material response, which will then have significant effects on the propagation of waves through these layered and graded structures.

4. Applied loading

Identical impulsive loadings are applied to all of the layered/graded structures considered. The loading consists of a uniform pressure applied on the top surface over a radius a ($a < h$); in the cases presented here, $a = 5.8$ mm. This pressure has the following variation with time (Fig. 5): a linear ramp to a maximum

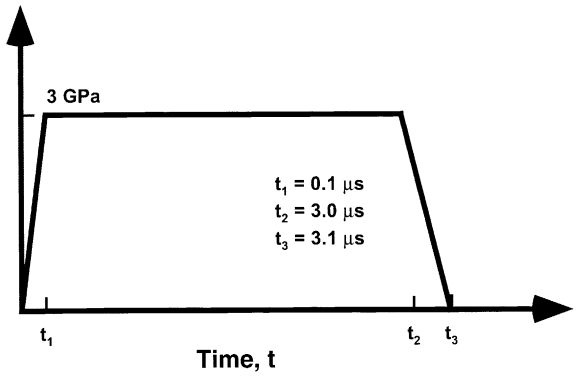

Fig. 5. History of impulsive loading applied on the top surface of the plates. The maximum applied pressure is 3 GPa.

pressure of 3 GPa over a rise time of 0.1 μs, followed by a dwell at the maximum pressure for 2.9 μs, and then a linear unloading to zero pressure over an additional time of 0.1 μs. The magnitude of the maximum applied pressure was chosen to be comparable to that expected during a representative armor impact event, and is large enough to ensure that plastic deformation will occur within the structure. The duration of the loading was chosen such that the effect of the unloading from the top surface can be initially decoupled from the effect of reflections from the bottom surface. The rise and fall times are chosen to be much larger than the transit times across any given reinforcement particle in the experimental structure, so that an effective medium approach remains a reasonable approximation.

5. Finite element model

The ABAQUS/Explicit finite element package was used to compute the response of the layered and graded plates to the prescribed impulsive loading. The problem is formulated as an elastic–viscoplastic nonlinear dynamic initial boundary value problem. An axisymmetric model is used, with 210 elements along the thickness direction. For the layered structure, the number of elements in each layer matches the thickness of that layer. For the graded cases, the variation in material properties along the thickness is discretized into 21 steps, so that every ten element layers have the same material properties. Representations of the meshes used for the layered case are shown in Fig. 6(a), and that used for the graded cases is shown in Fig. 6(b) (it is impossible to adequately represent 210 element layers within such Figures). We have examined the mesh dependence of our results for all of the cases (the worst case is Case B, where the top surface is soft matrix material and develops very large plastic deformations), and have established that the current meshes are sufficiently fine to capture all of the primary features of interest with acceptable accuracy.

6. Computational results

The general solution of such problems consists of determining all of the stresses and deformations at every point in the structure for all times. Both histories and distributions are significant for the dynamic problem; the interaction of waves usually determines where and when specific events occur, and thus the solutions are strongly dependent on the particular structures involved. The issues of greatest interest in the use of layered or graded structures for armor applications are quite specific:

- What are the maximum tensile stresses, and where and when do they occur? This is particularly important for determining whether or not spallation or debonding will occur in the structure.
- What is the distribution of the accumulated plastic strains at any given time, and what is the maximum plastic strain that is developed? This relates to the energy that is dissipated, as well as to the likelihood of being able to survive a second impact.
- What is the effect of the layering or gradation on these maxima and distributions? Is there some advantage to be gained from the development of the layering or gradation?
- What is the history of the kinetic energy, plastic dissipation and elastic strain energy for each structure?

These questions are explored in the subsequent sections. The fact that the magnitude of the loading applied is so large that plasticity is developed very quickly must be remembered while considering these results.

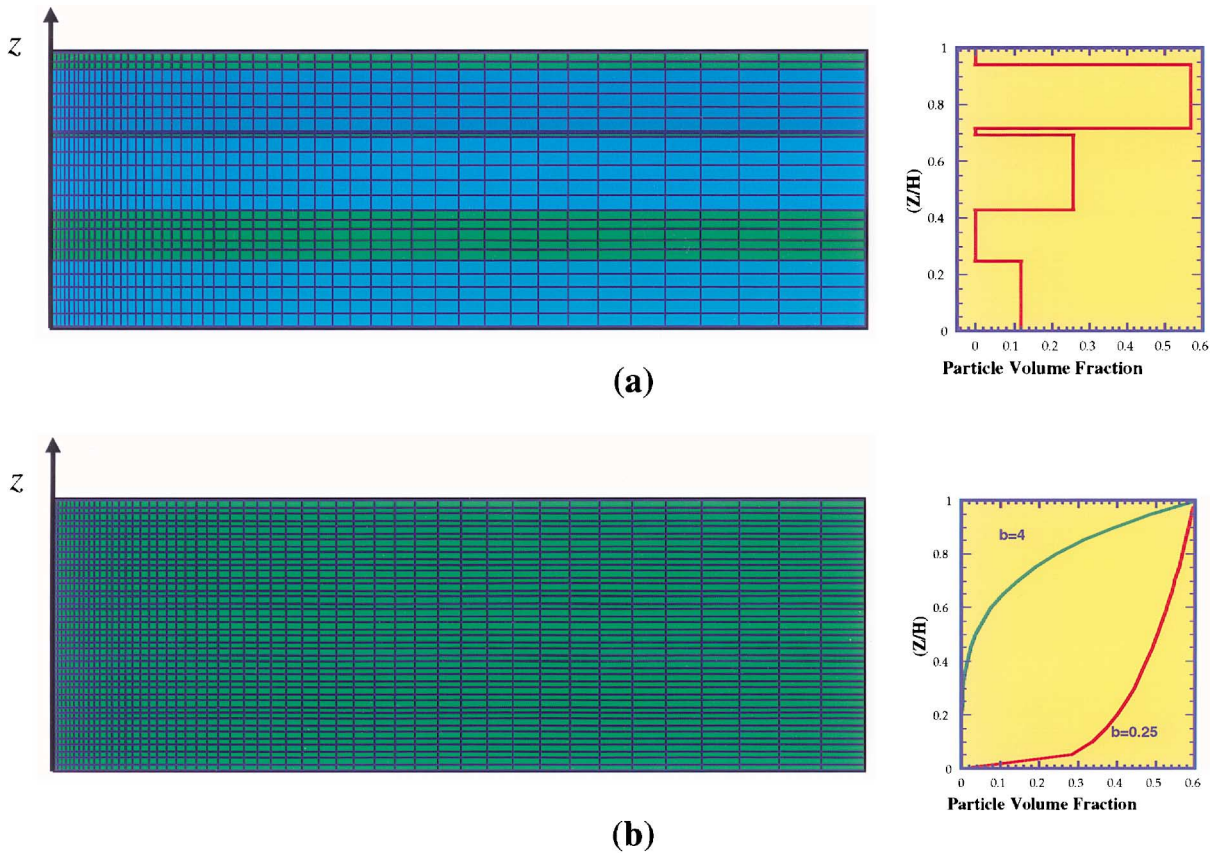

Fig. 6. Finite element meshes used for the simulations (one-half of the axisymmetric problem is shown, with the axis of symmetry on the left): (a) representation of mesh used for the layered structure (an identical mesh is used for the uniform Case A), and (b) representation of mesh used for the two graded structures. The actual mesh is too fine to display in this format (see text).

6.1. Axial stress distributions

The normal stress in the loading direction (S_{22} in the simulations, 2 being the direction of the plate normal) is of considerable interest to such armor plate problems, since a sufficiently large magnitude of tensile stress in this direction (particularly as a result of unloading from free surfaces) may result in spall and debond failures. For the uniform case (Case A), the initial compressive pulse developed by the applied compressive loading will propagate into the plate and reflect from the free bottom surface as an unloading wave, generating a tensile stress state just behind the free surface (possibly leading to spallation). The transit time across the thickness of the plate in this case is about 3 μs for the fastest elastic wave, so that the tensile stresses will be developed only at times greater than 3 μs after the initiation of the loading.

Contours of the Cauchy stress component S_{22} 4 μs after loading begins (a time at which tensile stresses may be expected) are shown in Fig. 7 for Cases A to D (blue stresses are compressive, and green-to-red stresses are tensile). Consider first Case A (the uniform material). Tensile stresses are observed near the rear free surface as a result of unloading, but the magnitudes of tension observed are small. In contrast, the identical loading has generated extremely high tensile stresses near the front surface in the layered structure (Case B), as a result of the interactions between reflections in the high-volume-fraction layer and the

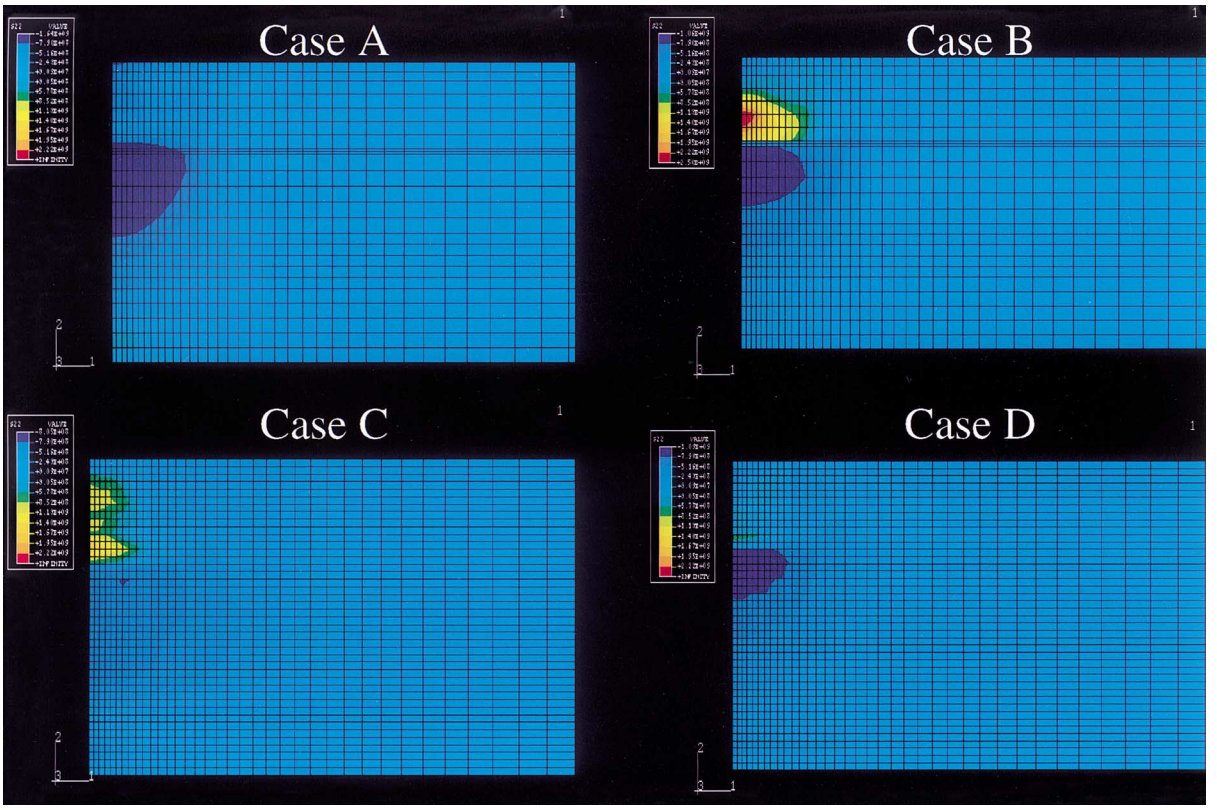

Fig. 7. Computed distributions of the S_{22} component of the Cauchy stress for each case 4 μs after commencement of the loading. Purple and blue colors represent compression, and green to red colors represent tension. Note the high tension near the top surface in Case B.

unloading at the top surface (note that unloadings can occur at each sudden impedance reduction and both at the top and bottom surfaces). Cases C and D (the two graded structures) show quite different distributions, with higher tensile but lower compressive stresses evident in Case C. Fig. 7 shows that the presence of the gradations and the layering have a dramatic impact on the tensile stress distributions (and therefore on the probability and location of tensile failures).

The time history of the stress component S_{22} along the axis of axisymmetry is presented in Fig. 8 for a sequence of times and for each of the four cases (Figs 8a–d correspond to Cases A–D respectively). Note that the right-hand edge of these plots represents the top or loading surface ($z = h$), while the left-hand edge represents the bottom or free surface; initial wave propagation is from right to left. Consider first the distributions in each case at a time of 3 μs (just before unloading begins at the top surface): these are the solid curves in Fig. 8. The compressive peak (the elastic precursor) that is evident near the rear surface has different amplitudes and occurs at different locations in each case, as a result of the dispersion inherent in these structures. Note that the waves are generating plastic deformations and so these wave amplitudes cannot be described in terms of elastic wavefronts; further, energy is also being radiated away along the plate. Note that at 3 μs the loading stress wave has not reached the rear surface in any case, so that the entire region from the top surface to the stress wave front is under compression at this time. At later times (e.g. 4 μs) the compressive loading peak reflects from the free surface as a tensile peak propagating to the right (or towards the top) into the pre-compressed region, while the unloading stress wave front from the

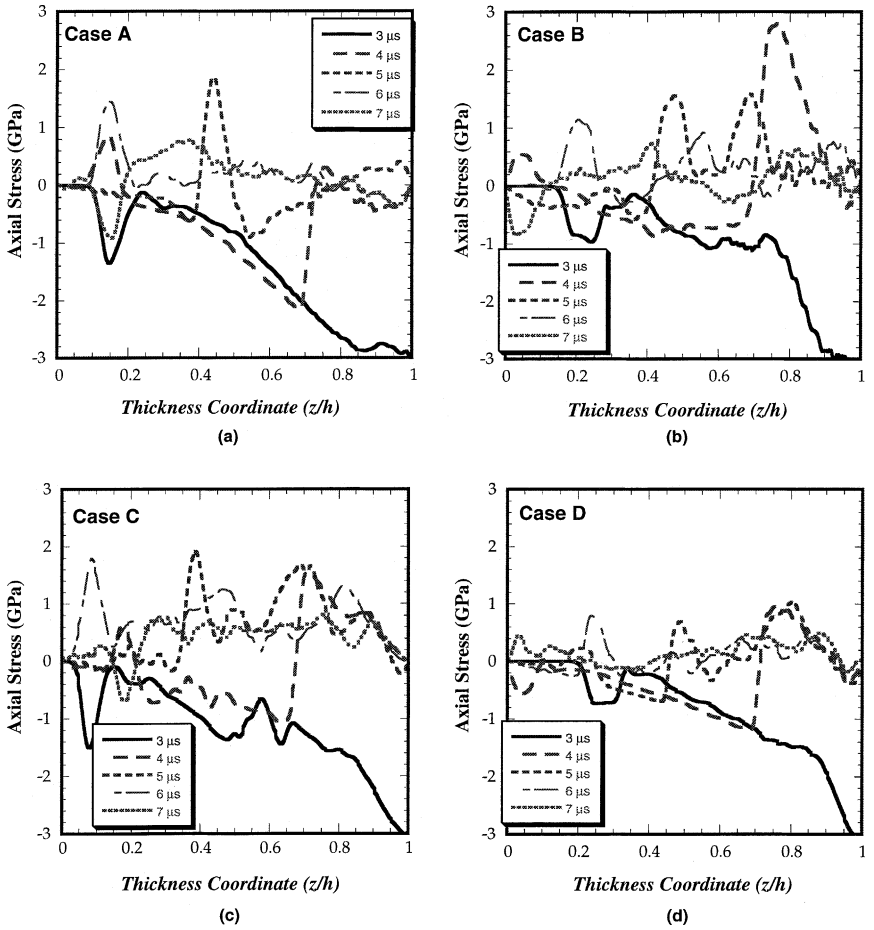

Fig. 8. Distributions of the stress component S_{22} along the axis of the plate in the thickness direction at various times after loading begins, for each of the four cases. The distributions at 4 μs correspond to the distributions (along the axis) shown in Fig. 7.

top surface propagates into the structure towards the left (or the bottom), reducing the stress to zero behind it (in Case A). The stress distributions in Case A can be easily understood in these terms. Thus the distribution at 4 μs in Case A shows the tensile peak reflected from the rear surface and the unloading to zero propagating in from the top surface (the full field distribution of S_{22} at this time is that shown in Fig. 7(a)). At a later time (5 μs) these two waves interact to generate the large tensile peak, and at later times still they pass each other and begin to interact with the bounding surfaces, resulting in the distributions shown in Fig. 8(a) for times of 6 and 7 μs.

The stress distributions developed in the layered structure of Case B (Fig. 8b) are much more complex, because of the multiple interactions of reflections from each of the layers, with the signs of the reflections dependent on the relative impedances of the adjacent layers. The stress distribution is quite different even at 3, and 4 μs an extremely large tensile peak is developed near the top surface (when the unloading wave propagating in from the top surface interacts with the tensile reflection from the bottom of the high-volume-fraction layer. This strong tensile stress may lead to spallation and debonding failures on the loading side of this layered structure, rather than on the free surface side as would be expected for Case A. Thus the layering has a very strong influence on the dynamic response.

The stress distributions developed in the graded plates of Cases C and D are less dramatically different from Case A than is Case B, but they are significantly different none the less. Note the slightly higher effective wavespeed in Case C, and the slightly lower effective wavespeed of Case D. Case C shows fairly strong tensile regions, while Case D appears to develop less tension than even the uniform Case A.

Thus the choice of gradation directly affects the dynamic response of these structures, and has strong implications for the potential failure modes. These results indicate that there are significant opportunities awaiting the engineer who attempts to design armor structures with graded or layered components, perhaps with the ability to control the likely failure mode.

6.2. Plastic strain distributions

The equivalent plastic strain provides a good measure of the extent of plastic deformation that is developed within each structure as a result of the dynamic loading. Distributions of the equivalent plastic strain along the axis of axisymmetry are shown in Fig. 9 for each of the four cases (Fig. 9a–d correspond to

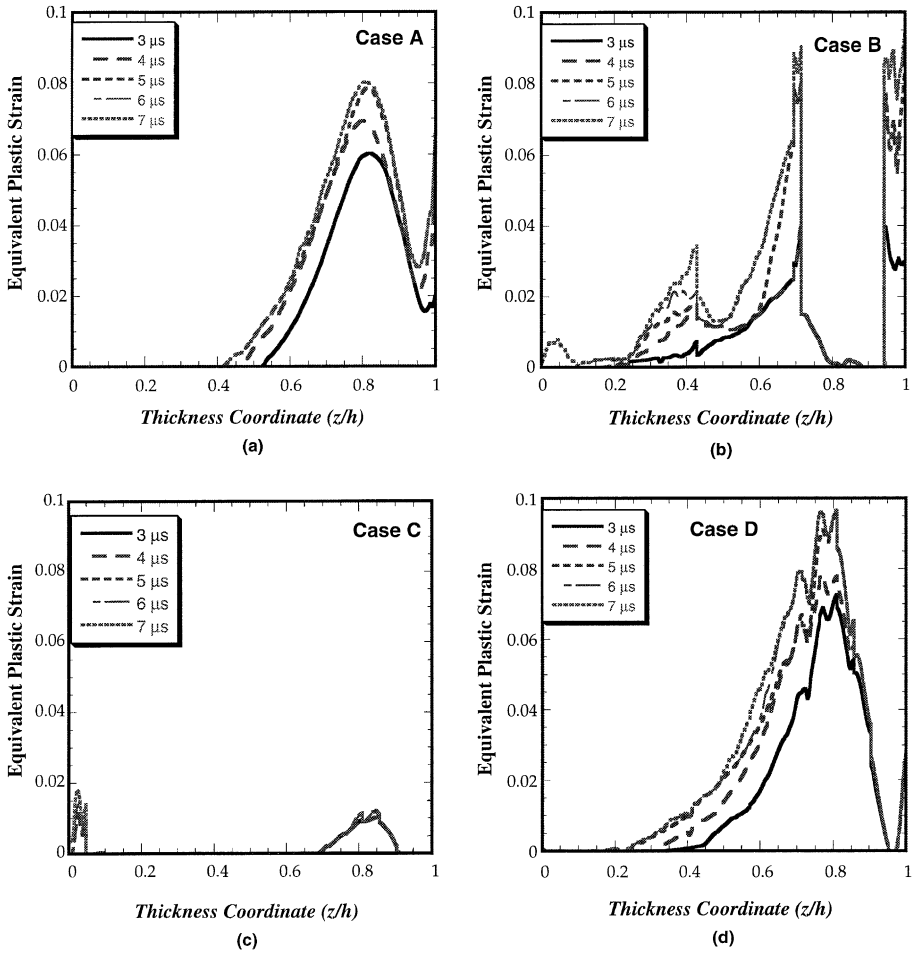

Fig. 9. Distributions of the equivalent plastic strain along the axis of the plate in the thickness direction at various times after loading begins, for each of the four cases. Note in particular the substantial differences between Cases A and B.

Cases A–D respectively) for the same sequence of times presented in Fig. 8. As in Fig. 8, the right-hand edge of each plot represents the impact face. In the uniform plate (Fig. 9a), most of the plastic strain is developed at about 20% of the depth (the minimum in the plastic strain distribution just below the surface is a result of the stress state associated with the pressure loading). The plastic strain accumulates rapidly for the first 5 μs, growing in magnitude and in the size of the plastic zone. However, very little change occurs after 5 μs, so that the subsequent stress waves are predominantly in the elastic range. In contrast, the equivalent plastic strain in the layered structure (Fig. 9b) is much more distributed, with the pure matrix layers developing very large plasticity and with substantial plastic deformation in the softer layers deep within the structure. The wave reflections in the layered structure also result in continued evolution of the plastic strain distribution even after 7 μs. The two graded structures (Cases C and D) show very different distributions. However, the mean reinforcement volume fraction in Case C is much higher than that in Case D, accounting for the smaller amounts of plastic deformation in C. Note that the decreasing strength of the material (Fig. 4d) with thickness in Case C results in substantial plasticity at the rear surface of the plate, even though the stresses developed there by the loading are quite small. Case D strongly resembles the uniform material (Case A) in terms of plastic strain development, although the plastic zone developed is somewhat larger in Case D.

The plastic strain distributions may have implications for the dynamic failure of these layered structures. Damage through particle fracture has been shown to develop within some particle-reinforced MMCs subjected to compressive stress states (Li et al., 2000b, Prangnell et al., 1996). The development of such compressive damage appears to be related to the magnitude of the overall plastic strain. Once the particles are fractured, the overall tensile strength of the material will be severely degraded. A region of the impacted structure that has first undergone plastic deformations (with the associated particle damage) may fracture if a sufficiently high tensile stress is subsequently developed in that region. Thus, an estimate of the likelihood of tensile failure in any particular region at any specific time may be obtained by considering the extent of prior plastic strain and the magnitude of the instantaneous tensile stress. Control of the plastic strain distribution and tensile stress history through appropriate layering and gradation may afford additional opportunities for controlling the failure mode, failure location, and failure time while retaining high structural stiffness.

6.3. Evolution of dissipated, kinetic and strain energies

The time evolution of the total dissipated energy, elastic strain energy and kinetic energy in the system has also been computed for these graded and layered structures. These energy estimates provide a useful way of comparing the ability of these structures to sustain dynamic loading. The external work is changed into energy dissipated in the viscoplastic deformations, kinetic energy and elastic strain energy. We examine the evolution of these energies with time after the loading begins, presenting each energy quantity normalized by the external work (these normalized quantities are referred to as energy fractions). In making these comparisons, note that the impulse begins to unload after 3 μs, and that Case C is significantly stiffer than the other cases because of the high mean volume fraction of reinforcement.

The dissipated energy fractions for the four cases are presented in Fig. 10(a). There is very little energy dissipated by Case C, corresponding to the small plastic strains developed in that structure (Fig. 9c) as a result of the very high yield stresses associated with the high mean volume fraction. The largest fraction of the external work is dissipated by Case B, the layered structure, with much of the gain (in comparison to the uniform Case A) developing at late times. The equivalent plastic strain distributions (along the axis of symmetry) shown in Fig. 9 indicate that much of the viscoplastic deformations in Case B occur in the pure metal layers. Case D initially dissipates less energy than Case A, but eventually is just about as effective at dissipation. The time delays observed in the development of dissipation in Cases C and D are a result of the very high yield stresses of the material at the top surface, so that the loading needs to propagate into the

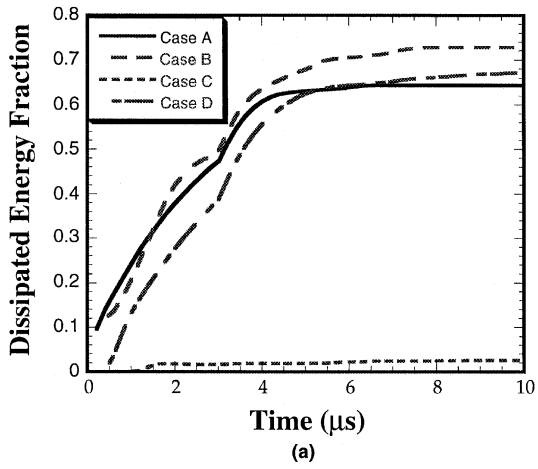

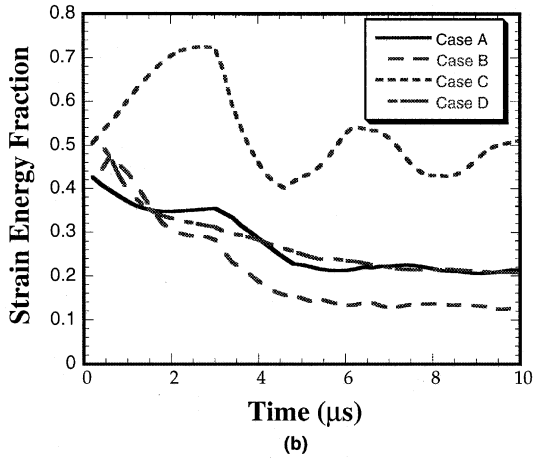

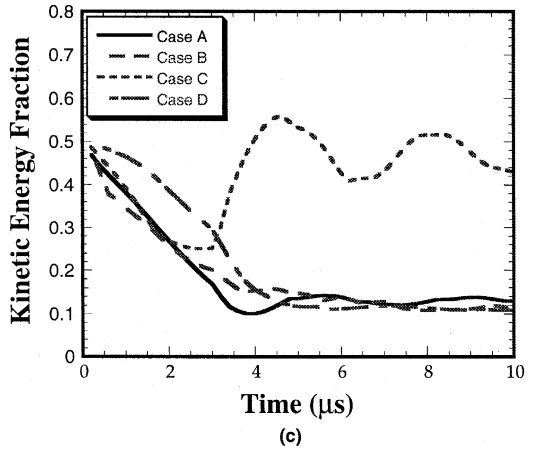

Fig. 10. Energy fractions (energy normalized by external work) as a function of time for each of the four cases. (a) Dissipated energy fraction; (b) elastic strain energy fraction and (c) kinetic energy fraction.

graded structures for some distance before plastic deformations are developed. Note in all these cases that the viscoplastic deformations are driven by the deviatoric stresses in this model, so that the largely compressive states directly below the loading circle develop little plasticity.

The elastic strain energy fractions are presented in Fig. 10(b) and the kinetic energy fractions in Fig. 10(c). The kinetic energy fractions are similar in Cases A, B and D after 4 μs, but the strain energy fractions show differences that are a direct result of the differences in dissipation presented in Fig. 10(a). The results for Case C are also a direct result of the small viscoplastic dissipations in this relatively hard structure: most of the energy is present as either strain energy or kinetic energy. The complementary oscillations in these energies are the classical representation of the propagation of stress waves within the structure.

These comparative studies of the energy evolution in these structures show that design of layering and gradation may be useful also for the control of the time evolution of the various energy fractions (an approach of some value in the applications of impact-tolerant structures). It should be noted, however, that the current computations do not evaluate the energies dissipated as a result of the damage that is likely to occur within such heterogeneous materials, and so these results are likely to be underestimates of the real dissipation. Computations involving damage and damage evolution are currently underway, and will be presented in a forthcoming publication.

7. Discussion and conclusions

There are several issues that are unique to the dynamic problem for graded and layered structures. A fundamental issue is the coupling of wavespeeds and timescales to length scales. If a volume fraction parameter alone is to be used to describe the gradation, it is necessary that the shortest rise time (t_r) in the problem be larger than the ratio of the reinforcement dimension (d_r) to the fastest wavespeed (c_r) in the reinforcing material, i.e., one must have $t_r \gg d_r/c_r$. In this work, the assumed rise time of 100 ns and a typical longitudinal wavespeed in a ceramic reinforcement of 10,000 $m\,s^{-1}$ implies that the largest reinforcement particle sizes allowable are of the order of a 100 μm. These particle sizes become a serious issue at the larger volume fractions, since an effective way to fabricate composites with high reinforcement volume fractions is to use bimodal particle size distributions for better packing. The lengthscale–timescale coupling also extends to structural length scales, so that different regimes of behavior may be developed in structures with different physical size scales.

Macroscopic interfaces are important in the dynamic problem for graded and layered structures in several special ways. Acoustic and shear impedance changes at interfaces control the reflection and refraction of stress waves through the structure, and may play a role in focusing or diverging the waves. Further, Stoneley waves propagating along interfaces may play a part in determining the dynamic response of the structure. Finally, the dynamic failure of interfaces may dominate the failure modes of the structure. However, unlike the quasistatic case, it is not generally clear that the elimination of interfaces through gradation will improve structural integrity under dynamic loading. Indeed, these simulations show that the reflections that occur off sharp interfaces can be used to control the probability and location of failures.

The most significant feature of these problems is the time evolution of the field quantities as a result of wave propagation and wave interactions with boundary conditions, interfaces and gradients. Dispersion of waves as a result of gradations of material behavior can be important, as in Cases C and D, resulting in either a compression or a spreading of the propagating pulses. Further, viscoplastic effects that arise from the gradation (e.g. Fig. 4d) may be extremely significant in dynamic problems such as armor involving large-amplitude loading. The great complexity of these problems is only just beginning to be explored, and unlike the quasistatic case, there are few examples in nature to provide guidance. The structural and topological optimization problem involving dynamic loadings remains one of the great open problems in mechanics, albeit with niche applications.

The primary results of this work are summarized below. The problem of the impact response of graded and layered structures has been explored for the first time, with specific reference to possible applications in armor structures. Computational predictions of the impact response are made, using as material inputs experimentally verified constitutive laws for the viscoplastic response of particle-reinforced MMCs (Li and Ramesh, 1998). Comparisons are made between the response of uniform (nongraded) structures, a physically realized layered structure and two model graded structures to impulsive pressure loading within an axisymmetric plate geometry. The following specific conclusions may be drawn from these results:

(1) Interfaces play a crucial role in these dynamic problems, and sharp or discontinuous interfaces may have strong value in structural design.

(2) Wave propagation within these graded and layered structures involves a complex coupling of elastic and viscoplastic responses. A full understanding of the local viscoplastic behaviors of the composite materials integrated into these structures is therefore a necessary precursor to such analyses. In this instance, such an understanding had already been developed through prior experimental and modeling efforts.

(3) The gradation or layering of the reinforcement volume fraction has a very significant impact on the axial stress distributions, and may be particularly useful in controlling the location and timing of spall failures. Proper gradation can cause spall failures to occur either near the impact face or near the rear face, and the magnitude of the local tensile stresses can be controlled.

(4) Gradation or layering of the reinforcement volume fraction also has an effect on the equivalent plastic strains that are developed in the impacted structure, so that the magnitude of the maximum plastic strain, the location and timing of this maximum, and the extent of the overall plastic zone can all be controlled by the appropriate choice of gradation or layering.

(5) The evolution of the dissipated energy and strain energy fractions with time are directly related to the gradation of material properties. This approach to evaluating the performance of impacted structures indicates that gradation and layering provide additional opportunities for optimization of performance.

Acknowledgements

This work was supported by the US Army Research Office under grant no. DAAH04-95-2-0006 and by the US Army Research Laboratory through grant no. DAAL01-96-2-0047. The authors wish to acknowledge discussions with K.J. Hemker of Johns Hopkins.

References

Finot, M., Suresh, S., 1996. Small and large deformation of thick and thin-film multi-layers: effects of layer geometry, plasticity and compositional gradients. J. Mech. Phys. Solids 44 (5), 683–721.

Finot, M., Suresh, S., Bull, C., Sampath, S., 1996. Curvature changes during thermal cycling of a compositionally graded Ni–Al_2O_3 multi-layered material. Mater. Sci. Engng. A205, 59–71.

Giannakopoulos, A.E., Suresh, S., 1997a. Indentation of solids with gradients in elastic properties: Part I. Point force. Int. J. Solids Struct. 34 (19), 2357–2392.

Giannakopoulos, A.E., Suresh, S., 1997b. Indentation of solids with gradients in elastic properties: Part II. Axisymmetric indentation. Int. J. Solids Struct. 34 (19), 2393–2428.

Ilschner, B., 1996. Lessons learnt in 7 years of FGM research at Lausanne. Functional Graded Materials 1996, Proceedings of the 4th International Symposium on Functionally Graded Materials, Elsevier, Tsukuba, Japan, pp. 15–20.

Li, Y., Ramesh, K.T., 1998. Influence of particle volume fraction, shape and aspect ratio on the behavior of particle-reinforced metal–matrix composites at high rates of strain. Acta Materialia 46 (16), 5633–5646.

Li, Y., Ramesh, K.T., Chin, E.S.C., 2000a. The compressive viscoplastic response of an A359/SiCp metal–matrix composite and of the A359 aluminum alloy matrix. Int. J. Solids Struct. 37, 7547–7562.

Li, Y., Ramesh, K.T., Chin, E.S.C., 2000b. Viscoplastic deformations and compressive damage in an A359/SiCp metal–matrix composite. Acta Materialia 48, 1563–1573.

Miyamoto, Y., Niino, M., Koizumi, M., 1996. FGM research program in Japan – from structure to functional uses. Functional Graded Materials 1996, Proceedings of the 4th International Symposium on Functionally Graded Materials, Elsevier, Tsukuba, Japan, pp. 1–8.

Mortensen, A., Suresh, S., 1995. Functionally graded metals and metal-ceramic composites: Part 1. Processing. Int. Mater. Rev. 40 (6), 239.

Pettermann, H.E., Weissenbek, E., Suresh, S., 1996. Simulation of the elastic–plastic deformations in compositionally graded metal-ceramic structures: mean-field and unit cell approaches. Functional Graded Materials 1996, Proceedings of the 4th International Symposium on Functionally Graded Materials, Elsevier, Tsukuba, Japan, pp. 75–80.

Prangnell, P.B., Barnes, S.J., Roberts, S.M., Withers, P.J., 1996. The effect of particle distribution on damage formation in particulate reinforced metal matrix composites deformed in compression. Mater. Sci. Engng. A220, 41–56.

Rabin, B.H., Williamson, R.L., Drake, J.T., 1993. Finite element analysis of thermal residual stresses at graded ceramic-metal interfaces: Part II. Interface optimization for residual stress reduction. J. Appl. Phys. 74 (2), 1321–1326.

Ravichandran, K.S., 1995. Thermal residual stresses in a functional graded material system. Mater. Sci. Engng. A201, 269–276.

Reiter, T., Dvorak, G., 1998. Micromechanical models for graded composite materials: II. Thermomechanical loading. J. Mech. Phys. Solids 46 (9), 1655–1673.

Reiter, T., Dvorak, G., Tvergaard, V., 1997. Micromechanical models for graded composite materials. J. Mech. Phys. Solids 45 (8), 1281–1302.

Rodel, J., Neubrand, A., 1996. Research program on gradient materials in Germany. Functional Graded Materials 1996, Proceedings of the 4th International Symposium on Functionally Graded Materials, Elsevier, Tsukuba, Japan, pp. 9–14.

Suresh, S., Mortensen, A., 1997. Functional graded metals and metal-ceramic composites: Part 2. Thermomechanical behavior. Int. Mater. Rev. 42 (3), 85.

Weissenbek, E., Pettermann, H.E., Suresh, S., 1997. Elastic–plastic deformation of compositionally graded metal-ceramic composites. Acta Mater. 45 (8), 3401–3417.

Williamson, R.L., Rabin, B.H., Drake, J.T., 1993. Finite element analysis of thermal residual stresses at graded ceramic–metal interfaces: Part I. Model description and geometrical effects. J. Appl. Phys. 74 (2), 1310–1320.

Yadav, S., Chichili, D.R., Ramesh, K.T., 1995. The mechanical response of a 6061-T6 Al/Al_2O_3 metal matrix composite at high rates of deformation. Acta Metall. Mater. 43 (12), 4453–4464.

Yang, Y.Y., Munz, D., 1995. Reduction of the stresses in a joint of dissimilar materials using graded materials as interlayer. Fract. Mech. (ASTM STP 1256) 26, 572–586.

Yang, Y.Y., Munz, D., 1996. Stress analysis in a two materials joint with a functionally graded material. Functional Graded Materials 1996, Proceedings of the 4th International Symposium on Functionally Graded Materials, Elsevier, Tsukuba, Japan, pp. 41–46.